Electronic Supporting Information for

A solid-state integrated photo-supercapacitor based on ZnO nanorod arrays decorated with Ag_2S quantum dots as photoanode and PEDOT charge storage counter-electrode

Daniel Solís-Cortés[a], Elena Navarrete-Astorga[a], Ricardo Schrebler[c], Juan J. Peinado-Pérez[a], Francisco Martín[a], José R. Ramos-Barrado[a] and Enrique A. Dalchiele[b].

a Universidad de Málaga. Andalucía Tech. Departamentos de Física Aplicada & Ingeniería Química. Laboratorio de Materiales y Superficies (Unidad Asociada al CSIC), E29071 Málaga, Spain.

b Instituto de Física, Facultad de Ingeniería, Herrera y Reissig 565, C.C. 30, 11000 Montevideo, Uruguay.

c Instituto de Química, Facultad de Ciencias, Pontificia Universidad Católica de Valparaíso, Casilla 4059, Valparaíso, Chile

1. Characterization of the Ag_2S/ZnO NRs photoelectrode

Figure S1 shows a typical X-ray diffraction pattern of ZnO nanowire arrays (blue line) and ZnO nanowires covered with Ag_2S QDs (red line) for comparison. The X-ray diffraction peaks can be indexed as monoclinic Ag_2S structure (JCPDS file No. 00-014-0072). It can be appreciated that the obtained Ag_2S QDs/ZnO nanowires arrays share the structural characters of both ZnO and Ag_2S because no any other diffraction peaks besides SnO_2 which comes from the FTO substrate were detected.

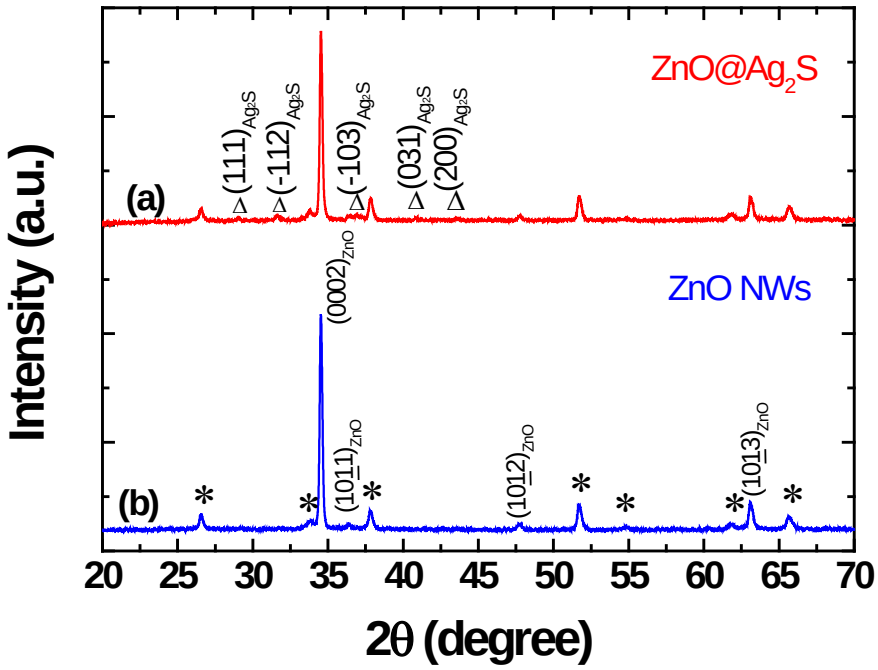

Figure S1. X-ray diffraction pattern of (a) ZnO sensitized Ag_2S QDs (JCPDS 14-0072) and (b) ZnO nanowire. Diffraction planes are indicated for ZnO and Ag_2S. (*, indicates the peaks originated from the SnO_2:F substrate).

On the other hand, five diffraction peaks at 29º, 31.5º, 37.7º, 40.7º and 43.3º corresponding to the (111), (-112), (-103), (031) and (200) planes respectively, of the acanthite crystal of Ag_2S, can be appreciated. The diffraction peak intensity of ZnO shows a little decrease after depositing Ag_2S QDs due to the ZnO NRs were completely covered with Ag_2S.

2. Characterization of the [HEMIM][BF_4]/PVP electrolyte.

The ionic conductivity of electrolytes depends on the number of mobile charge species and their mobility along with polymer chain mobility. The room-temperature ionic conductivity of [HEMIm][BF_4]/PVP electrolyte is σ = 1.5 10^{-3} S cm^{-1}, which is comparable to the neat [HEMIm][BF_4] ionic liquid that is 4.6 10^{-3} S cm^{-1} at 25 ºC.[1,2] However, pure PVP is highly resistive with $\sigma < 10^{-9}$ S cm^{-1}.[3]

The dependence between temperature and ionic conductivity is represented in Fig. S2. As can be observed in Fig. S2 (a), the ionic conductivity increases exponentially with temperature. This behavior is similar for other ionic liquids studied in literature.[4] Figure S2 (b) shows the natural logarithm of σ versus the inverse of absolute temperature, i.e., ln σ versus 1/T. If the electrolyte under study would follow a Vogel-Tamman-Fulcher (VTF) type equation, the data of Fig. S2 (b) had to form a curvature.[5,6] However, lnσ has a linear relationship with reciprocal temperature, following an Arrhenius relation, which can be written as:[7]

$$\sigma = \sigma_0 \exp\left[-\frac{Ea}{k_B T}\right] \qquad (eq.\ \text{S1})$$

where , σ_0 is the maximum electrical conductivity (that it would have at infinite temperature), E_a is the activation energy for electrical conduction, that indicates the

energy needed for an ion to hop to a free hole, k_B is the Boltzmann constant and T is the absolute temperature.

The increment of conductivity according to the temperature may be due to the reduction of viscosity and enhancement mobility of polymer chains. This linear behavior between conductivity and temperature is in agreement with the J. Tang *et al*.[8] research and it can be explained due to the free volume and the hopping of charge carriers between localized sites.[9] The crystallinity of the polymer at low temperatures is high and this succeed hinders the motion of ions, producing a decrease in the overall ionic conductivity. As the temperature rises, the amorphicity of the polymer increases gradually producing a segmental mobility of the polymer chains.[10,11] This amorphicity can promote inter and intra-chain ion hopping movements, leading to an increase in ionic conductivity.[12]

Red lines in Fig. S2 shows the best fitting, and from the linear fitting (Fig. S2 (b)) has been obtained the parameters of Arrhenius equation; σ_0 = 110.38 S cm^{-1} and E_a=0.28 eV. This low value of activation energy for ionic conduction is desirable for photo-supercapacitor applications.[13]

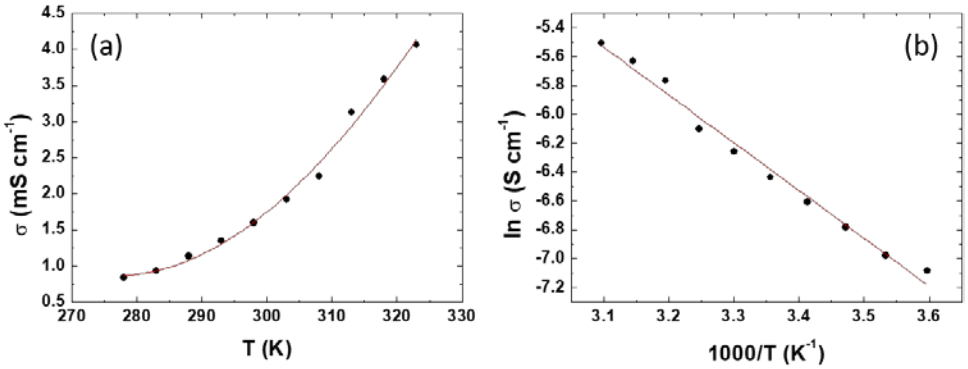

Figure S2 (a) Ionic conductivity, σ, as a function of absolute temperature and (b) Logarithm of the ionic conductivity versus the inverse of the absolute temperature for the PVP/[HEMIm][BF_4] electrolyte. Red lines are the best fit of the data.

3. Overall efficiency ($\eta_{overall}$) and storage effciciency ($\eta_{storage}$) of the photocapacitor

The $\eta_{overall}$ of the photocapacitor was calculated according to the equation eq. S2,[14] where E_{sp} is the specific energy, E_{light} the incident light power density (100 mW cm^{-2}) multiplied by the photocharge time and $A_{photocap.}$ the area of the photocapacitor (0.25 cm^2).

$$\eta_{overall} = \frac{E_{sp}}{E_{light} \cdot A_{photocap.}} \qquad (eq.S2)$$

On the other hand, the maximum storage efficiency $\eta_{storage}$ of the photocapacitor was calculated following the equation eq. S3,[15]

$$\mu_{storage} = \frac{\mu_{overall}}{\mu_{conversion}} \qquad (eq.\ S3)$$

where $\mu_{conversion}$ is the photovoltaic conversion efficiency that can be measured as follows.

$$\mu_{conversion} = \frac{V_{oc}J_{sc}FF}{P_{in}} \qquad (eq.\ S4)$$

where V_{oc}, J_{sc}, FF and P_{in} are the open circuit voltage, short-circuit current density, fill factor and incident light power density, respectively.

References

1 F. X., in *Polymer Electrolytes: Fundamentals and Applications*, eds. C. Sequeira and D. Santos, Woodhead Publishing Limited, 2010, p. 3.

2 S. Yeon, K. Kim, S. Choi, J. Cha and H. Lee, *J. Phys. Chem.*, 2005, **109**, 17928.

3 A. L. Saroj, R. K. Singh and S. Chandra, *Mater. Sci. Eng. B Solid-State Mater. Adv. Technol.*, 2013, **178**, 231–238.

4 J. Vila, P. Ginés, J. M. Pico, C. Franjo, E. Jiménez, L. M. Varela and O. Cabeza, *Fluid Phase Equilib.*, 2006, **242**, 141–146.

5 E. Navarrete-Astorga, J. Rodríguez-Moreno, E. A. Dalchiele, R. Schrebler, P.

Leyton, J. R. Ramos-Barrado and F. Martín, *J. Solid State Electrochem.*, 2017, **21**, 1431–1444.

6 K. H. Lee, S. Zhang, T. P. Lodge and C. D. Frisbie, *J. Phys. Chem. B*, 2011, **115**, 3315–3321.

7 J. O. Bockris and A. K. N. Reddy, in *Modern Electrochemistry*, Plenum Press, New York, 2nd edn., 1998, pp. 601–753.

8 J. Tang, R. Muchakayala, S. Song, M. Wang and K. N. Kumar, *Polym. Test.*, 2016, **50**, 247–254.

9 R. Nadimicherla, R. Kalla, R. Muchakayala and X. Guo, *Solid State Ionics*, 2015, **278**, 260–267.

10 C. A. Vincent, *Prog. Solid State Chem.*, 1987, **17**, 145–261.

11 J. E. Weston and B. C. H. Steele, *Solid State Ionics*, 1981, **2**, 347–354.

12 T. Miyamoto and K. Shibayama, *J. Appl. Phys.*, 1973, **44**, 5372–5376.

13 G. Hirankumar, S. Selvasekarapandian, M. S. Bhuvaneswari, R. Baskaran and M. Vijayakumar, *J. Solid State Electrochem.*, 2006, **10**, 193–197.

14 Y. Jin, Z. Li, L. Qin, X. Liu, L. Mao, Y. Wang, F. Qin, Y. Liu, Y. Zhou and F. Zhang, *Adv. Mater. Interfaces*, 2017, **4**, 1–8.

15 Y. Fu, H. Wu, S. Ye, X. Cai, X. Yu, S. Hou, H. Kafafy and D. Zou, *Energy Environ. Sci.*, 2013, **6**, 805–812.